About Equilibrium Mode Ruling Ferritic Transformation in Low-Alloy SGI

Laura Noel García, Fernando Diego Carazo & Roberto Enrique Boeri

Metallurgical and Materials Transactions A

ISSN 1073-5623
Volume 50
Number 12

Metall and Mat Trans A (2019)
50:5585-5593
DOI 10.1007/s11661-019-05485-6

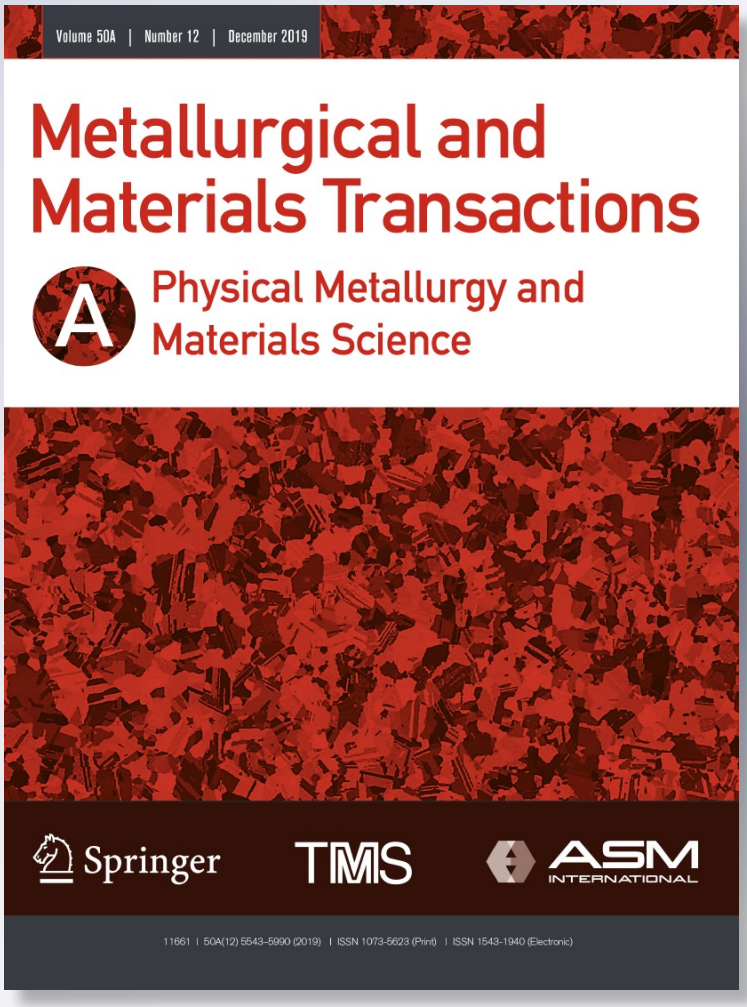

Springer

About Equilibrium Mode Ruling Ferritic Transformation in Low-Alloy SGI

LAURA NOEL GARCÍA, FERNANDO DIEGO CARAZO, and ROBERTO ENRIQUE BOERI

Ferrite precipitating around the graphite nodules shaping the typical bull's-eye microstructure could grow under negligible partitioning local equilibrium or under paraequilibrium conditions, as both imply that ferrite inherits the composition of the parent austenite. The first mechanism has been rejected by other researchers by means of simple calculations of the silicon spike width necessary for local equilibrium conditions to take place. Nevertheless, experimental analyses are necessary to verify this conclusion. In this study, transmission electron microscopy has been used to assess the presence of a silicon spike in front of the growing ferrite interface. The outcome allowed the authors to confirm that a paraequilibrium mode governs the transformation, supporting the conclusions of previous calculations. In addition, some issues about ferrite growth modeling are discussed.

https://doi.org/10.1007/s11661-019-05485-6

I. INTRODUCTION

SPHEROIDAL graphite cast iron (SGI) is a Fe-C-Si alloy in which free graphite precipitates in spheroidal or nodular shape. Under regular cooling conditions, its metal matrix microstructure consists of graphite nodules enveloped by ferrite halos and variable amounts of pearlite. This microstructure, known as bull's-eye ferrite (Figure 1), results from the solid-state transformations experimented by the austenite during its cooling at rates greater than 1.2 °C/min.[1,2]

The growth of ferrite is driven by *C* diffusion from austenite to graphite through the ferrite halo. At these cooling rates, no diffusion of substitutional elements has been reported to take place during austenite transformation[1] and the final microstructure, either ferrite or pearlite, inherits the microsegregation profiles developed during solidification. Lacaze *et al.*[1] described the ferrite precipitation by means of a stable Fe-C-Si isopleth section calculated for a nominal content of Si, as shown in Figure 2.

According to Lacaze *et al.*[1] once the temperature of the alloy drops below the upper limit of the ferrite/austenite/graphite ($\alpha + \gamma + G$) field $-T^{\upsilon}_{\alpha}-$, ferrite nucleates at the G/γ interface but cannot grow. Later on, it grows as spherical shells by diffusion of *C* from the austenite to the graphite through the ferrite halo. Consequently, ferrite growth can proceed only at temperatures below the lower limit of the three-phase field $-T_{\alpha}-$, when the *C* gradient given by the difference in the *C* concentration between the α/γ and the α/G interfaces turns to positive values.

A. *About Full and Partial Local Equilibrium*

The diffusion coefficient of *C* in austenite is known to be of the order of 10^6 times greater than the diffusion coefficient of the substitutional elements. Much has been claimed about the consequences of this difference in diffusivity on the precipitation at different temperatures. Coates[3] cast light on the effect of the alloying elements on the growth rate of a precipitate in ternary alloys; he described two growth modes: partitioning local equilibrium (PLE) and negligible partitioning local equilibrium (NPLE).

Assuming that the growth of pro-eutectoid ferrite in a ternary alloy takes place under the PLE mode, then the partitioning of the alloying elements between the ferrite and the austenite must take place. Consequently, the growth rate will be controlled by the diffusion rate of the slowest diffuser: the substitutional element. On the other hand, if the transformation is assumed to take place under NPLE regime, the C diffusion will control growth

LAURA NOEL GARCÍA and FERNANDO DIEGO CARAZO are with the CONICET, Godoy Cruz 2290, C1425FQB Buenos Aires, Argentina and also with the Instituto de Mecánica Aplicada, Universidad Nacional de San Juan, Av. Libertador Gral. San Martín 1109 (Oeste), J5400 San Juan, Argentina. Contact e-mail: lauranoelg@unsj.edu.ar. ROBERTO ENRIQUE BOERI is with the CONICET and also with the Instituto de Investigaciones en Ciencia y Tecnología de Materiales, Universidad Nacional de Mar del Plata-CONICET, B7608FDQ Mar del Plata, Argentina.

Manuscript Submitted July 19, 2019.
Article published online October 11, 2019

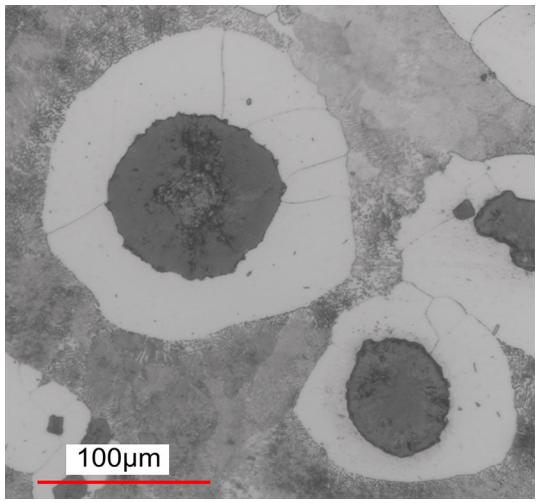

Fig. 1—Typical bull's-eye structure of the SGI.

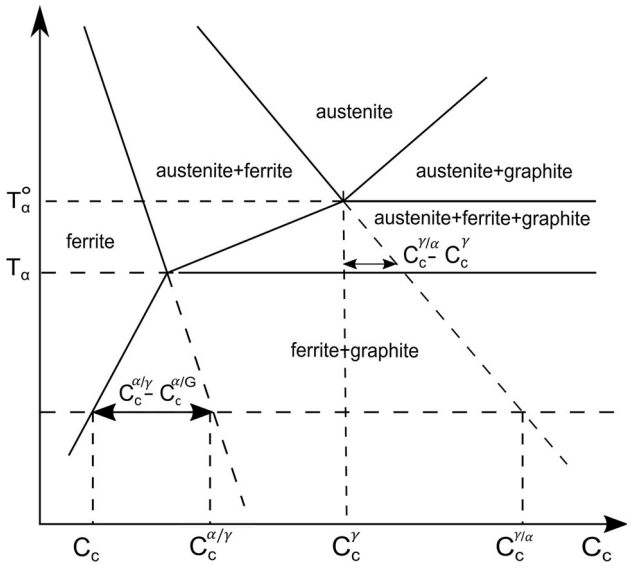

Fig. 2—Schematic representation of a stable Fe-C-Si isopleth section with a constant percentage of Si.

rate and therefore ferrite growth will be faster than in the former case.[3] The PLE/NPLE transition boundary (Figure 3) can be determined by a simple procedure.[3]

Although the substitutional element does not partition under the NPLE mode, the development of a spike of the alloying element in front of the growing interface is necessary for the local equilibrium to be maintained.[3] The spike is likely to be detected only at slow cooling rates. At high cooling rates, its thickness becomes so thin that it can be neglected and the NPLE mode is replaced by the paraequilibrium (PE) mode. In either case, the final structure inherits the alloying element concentration of the parent phase.

Finally, if ferrite precipitation is assumed to proceed under PE conditions, its growth will be dominated by the C diffusion and there will be no redistribution of alloying elements. The ferrite/austenite interface will be

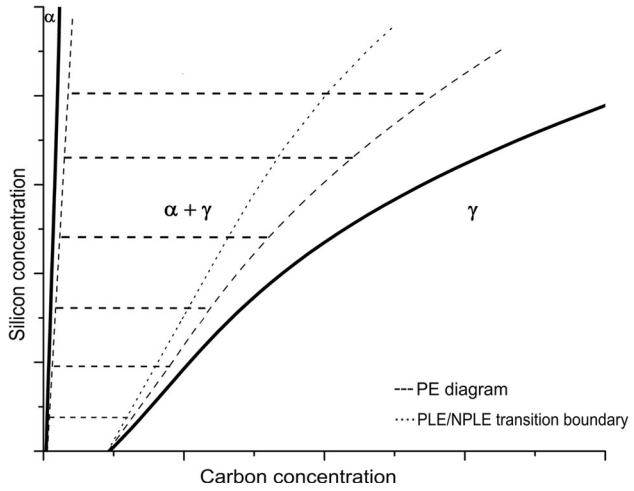

Fig. 3—Schematic representation of a stable Fe-C-Si isotherm section where the PLE/NPLE transition boundary is indicated. The PE diagram is overlapped.

in local equilibrium only with respect to the substitutional element. To represent these conditions, the equilibrium phase diagram has to be replaced by a PE diagram, where the tie-lines are horizontal, as shown in Figure 3.

B. *PLE/NPLE/PE Modes in SG Cast Irons*

Wessen and Svensson[4] made some simple calculations for estimating the thickness of the substitutional elements spike in austenite in contact with ferrite in case of ferrite growth under continuous cooling; they found that it was of the order of 10^{-11} m, less than an atomic distance. Thus, they concluded that a NPLE mode could not rule the austenite transformation in the case of SGI, but it has to proceed under PE.

Most of the authors have agreed on the fact that the decomposition of austenite in SGI develops with no partition of alloying elements.[1] Indeed, some authors have found a correspondence between the composition profiles measured on samples quenched directly from the solidification stage and those measured on the as-cast samples,[5] while others have simulated those developed during the solidification, arriving at the same conclusions.[6]

However, other authors, particularly Guo and Stefanescu[7] have concluded that partitioning of alloying elements during the solid-state transformations is possible. They performed wavelength-dispersive spectrometer measurement through the austenite/ferrite and austenite/pearlite interfaces in samples quenched from variable temperatures during the eutectoid transformation and found differences in the alloying concentrations through those interfaces. They concluded that Cr and Mn have positive segregation, while Cu and Si show negative segregation. Freulon *et al.*[8] dismissed these results and assumed that the concentration differences could be attributed to the microsegregation profiles inherited from the solidification step and to the

formation of carbides. This was discussed by Stefanescu[9] in a letter to the editor in which he claimed that although different interpretations could be suggested for the detected partitioning, the results could not be ignored. Stefanescu also neglected that the profiles could have been influenced by the presence of carbides. Lacaze replied to this letter[10] and he stated that the changes in Si content detected by Guo and Stefanescu were within the range of statistical variation associated with the employed characterization technique. Further, Lacaze pointed out that, as the analyses were carried out on etched samples, the small measured differences could hardly be considered for any quantitative use. Although the selected characterization technique might not be sensitive enough, the results of Guo and Stefanescu are conflictive and the matter deserves further analysis.

All studies considered, it can be inferred that the equilibrium mode governing ferrite growth in low-alloy SGI still represents a subject to be explored. Particularly, the partitioning of Si at the interface has not been thoroughly examined. In addition, it is worth noting that most studies recognized the potential influence of microsegregation on the precipitation of ferrite, but the actual Si concentration profile was not accounted for in the analysis. The microsegregation during the solidification of SGI has been characterized quantitatively by EDS and WDS examination, and qualitatively by color etching.[5,11] It has been shown that Mn, Cr, and Mo increase their concentrations towards the last liquid to solidify (LTF), while Si, Cu, and Ni are more concentrated at the solid formed first (FTF). Since SGI behaves as a divorced eutectic,[11] austenite and graphite nucleate and initially grow in the liquid independently. Nevertheless, as the austenite dendrites grow, they interact with graphite nodules, enveloping them. Therefore, the solute concentration of the austenite surrounding most graphite nodules corresponds to that at the FTF. As solidification advances, the austenite enveloping the nodules thickens, and its local chemical composition changes, developing a concentration profile. For example, greater Si concentration is usually found at the matrix surrounding the graphite nodules.

In this study, the simplest possible system is looked at, *i.e.,* the Fe-C-Si system, and the presence of other substitutional alloying elements is ignored. High spatial resolution EDS-TEM measurements of Si concentration through the austenite/ferrite interface were performed in order to investigate the presence of a spike. The longer-range Si microsegregation profile between nodules is accounted for in the discussion of the results.[12] This study is expected to clarify which mode rules ferrite growth around the graphite nodules (NPLE or PE) under continuous cooling conditions.

II. EXPERIMENTAL PROCEDURE

In order to develop this study, one ferritic SGI was cast. The melt was obtained in a medium-frequency induction furnace with a capacity of 1500 kg. SAE 1010 scrap, cast iron returns, pig iron, and graphite were used as raw materials. Ground graphite was added for the purpose of adjusting the C content, while Si_2Ca and FeSi were used for adjusting the Si concentration. Successively, the base metal was overheated to 1650 °C for 20 minutes, after what approximately 1.5 wt pct of Fe-Si-Mg-Ce was used as a nodulizing agent. The graphitization and inoculation processes were conducted using the sandwich method. In the reaction ladle, 0.7 wt pct of fine FeSi (75 wt pct Si) was added. Finally, the cast metal was poured into a ladle to fill Y-block-shaped green sand molds for obtaining 1-inch Y-blocks according to ASTM A536-84.[13]

The composition of the low-alloy SGI is listed in Table 1 and its microstructure is shown in Figure 4. The metal matrix is 82 pct ferritic.

The cooling rate was recorded, averaging 20 °C/min between 900 °C and 800 °C.

A. *Scanning Differential Calorimetry*

One disc-shaped sample was prepared to test it using a scanning differential calorimeter (DSC) at a cooling rate of 20 °C/min. This equipment was previously temperature and heat flux calibrated comparing to the temperature and fusion enthalpies of In, Sn, Al, and Ar. During the test, the temperatures of the sample and of the equipment were registered, as well as the heat flux as a function of time. An argon atmosphere of 30 ml/min was used at a constant pressure of 1 atm.

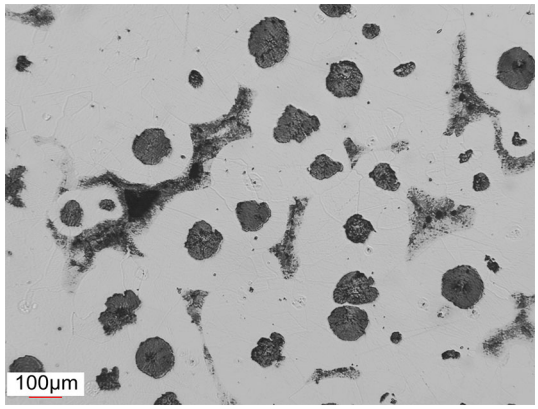

Fig. 4—Microstructure of the nearly fully ferritic SGI tested.

Table 1. Chemical Composition of the Alloy Studied in this Work

Element	C	Si	Mn	P	S	Cr	Cu	Sn	Mg	Al	CE
Concentration (Wt Pct)	3.67	2.8	0.21	0.038	0.01	0.025	0.01	0.009	0.041	0.012	4.70

CE refers to carbon equivalent.

The steps were the following:

1. Heating at 20 °C/min up to 950 °C.
2. Maintenance at 950 °C for 20 minutes.
3. Cooling at 20 °C/min.

The heating rate was arbitrarily chosen, as it has been demonstrated that it does not play any important effect on the recorded curves.[14] The austenitization time was selected so that the redistribution of C was possible.[2] The cooling rate was set to agree with the value measured during the cooling after the sample casting.

B. *Interrupted Quenching*

Interrupted quenching experiments were carried out using a dilatometer. Four new samples were prepared to be tested. The beginning-of-transformation temperatures found after analyzing the DSC curves were considered as a reference for the selection of the quenching temperatures to study the ferrite/austenite interface during ferrite growth.

The steps were the following:

1. Heating at 20 °C/min up to 950 °C.
2. Held at 950 °C for 20 minutes.
3. Cooling at 20 °C/min up to four different quenching temperatures: 775 °C, 760 °C, 745 °C and 730 °C.

Heating and holding stages were conducted under vacuum, while helium was used for quenching.

The samples were examined by SEM to check the advance of the ferrite transformation in each case.

C. *Transmission Electron Microscopy*

The quenched samples were studied making use of a FEI Tecnai F20 Transmission Electron Microscope (TEM) operated at 200 kV. This microscope is equipped with a Schottky field emission gun and an EDAX Apollo EDS for microanalysis with a spatial resolution of 1 nm.

Silicon point analyses were performed every 2 nm in a path crossing through the austenite/ferrite interface. Point measurements were also performed at different locations of the bulk. In the latter case, the concentrations were determined using the Cliff–Lorimer method with calculated k_{AB} factors. Due to the uncertainty in these factors, the results do not represent a reliable quantification[15] but are suitable for comparing the content of Si in each sample.

The preparation of the specimens involved a sequence of steps:

1. A 3-mm-diameter cylinder was machined from each block and sliced with a slow-speed diamond wheel saw.
2. The thickness of the discs was reduced to about 200 μm by mechanical grinding.
3. Thinning to achieve electron transparency was carried out by dimple grinding combined with ion milling using a Precision Ion Polishing System.

III. RESULTS AND DISCUSSION

The change in Si concentration between graphite nodules of the alloy investigated was measured in a previous work.[12] The results in Figure 5 show that Si concentration is higher at the ferrite in contact with the nodules and decreases as the distance from the nodule increases.

The DSC curve is plotted in Figure 6. Two stages of the solid-state transformations in SGI can be distinguished on the heat flux curve: at high temperatures, the starting of the ferritic transformation; at lower temperatures, the formation of pearlite.[2]

The SE images of the sample after quenching at different temperatures are shown in Figure 7. The advance of the ferritic transformation as a function of temperature can be distinguished: at 775 °C

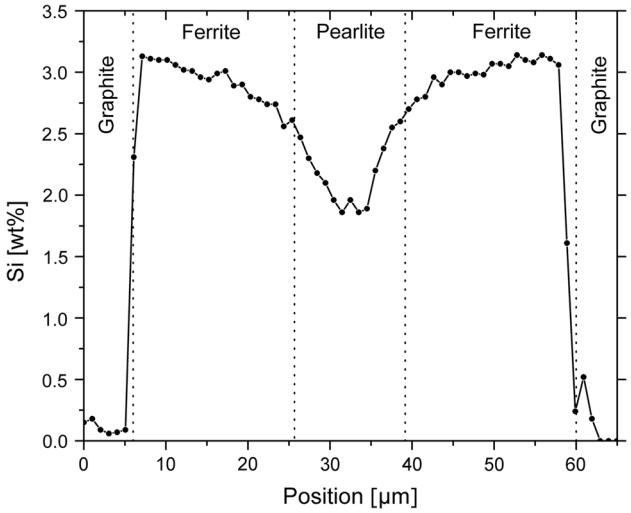

Fig. 5—Typical Si concentration profile between nodules in the alloy studied in this work. Adapted from García *et al.* results.[12]

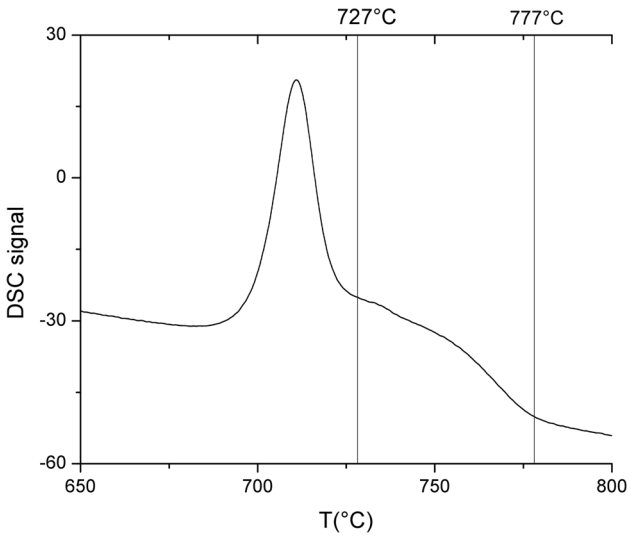

Fig. 6—DSC curve for a cooling rate of 20 °C/min.

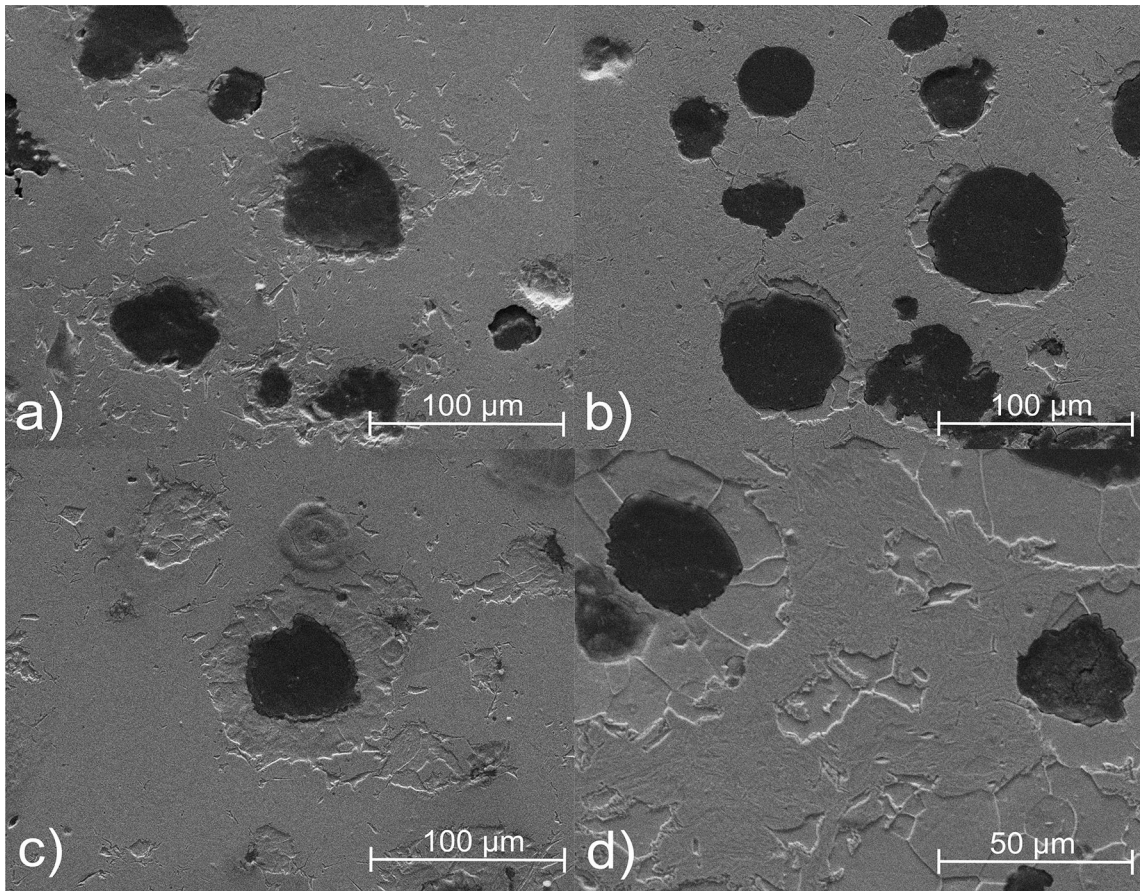

Fig. 7—SE images of the ferritic samples quenched making use of the dilatometer. The temperatures from which the samples were quenched are specified: (*a*) 775 °C; (*b*) 760 °C; (*c*) 745 °C; (*d*) 730 °C.

(Figure 7(a)) a very small amount of ferrite has nucleated around the graphite nodules. The remaining portion of the matrix is most probably martensite, as it results from the fast cooling of the austenite. As the temperature decreases (Figures 7(b) through (d)), the amount of ferrite increases progressively. Undoubtedly, at these temperatures, it is possible to find austenite/ferrite interfaces to carry out the Si-concentration measurements (martensite/ferrite at room temperature).

Figures 8, 9, 10, and 11 show bright-field TEM images of the ferrite/martensite interface, along with the Si intensity profiles. In each case, the line going through the interface indicates the path followed by the beam. In addition, point concentration measurements of Si are reported at different locations of the bulk, at both sides of the interface. It is clear that as the quenching temperature diminishes, and the fraction of ferrite increases, the average amount of Si around the ferrite/martensite interface diminishes. This verifies that the concentration of Si changes as the distance from the graphite nodules increases.

At high temperatures, the extension of the ferrite halo is minimal, so that the concentrations detected at the interface should be higher than those found at longer distances from the nodules, as Si tends to concentrate at the FTF (closer to the spheroids). As the transformation advances, it is expected that the interface moves towards the LTF, where lower concentrations of Si should be present.

The change in Si concentration across the ferrite/martensite interface is not marked at all, but for the sample quenched from 730 °C. Nevertheless, even for this latest case, the measured profile does not suggest the presence of a spike. The difference in intensity measured in Fig 11 can be caused by microsegregation generated during solidification.[5] In summary, the results do not support the presence of a Si spike at the austenite in front of the growing ferrite interface.

The fact that different Si concentrations are found as the transformation front advances added to the absence of a Si spike clearly demonstrates that the NPLE mode is not ruling the transformation.

Summarizing, during the transformation of austenite of SGI upon cooling, ferrite nucleates at the graphite/austenite interface and grows from this location, conforming nearly spherical units surrounding the graphite spheroids. The ferrite interface advance does not involve Si partition, and the ferrite inherits the Si concentration of the austenite. Consequently, it is not necessary to assume a chemically homogeneous matrix to describe the ferritic transformation making use of an isopleth section.[1] Instead, as a PE mode is governing the

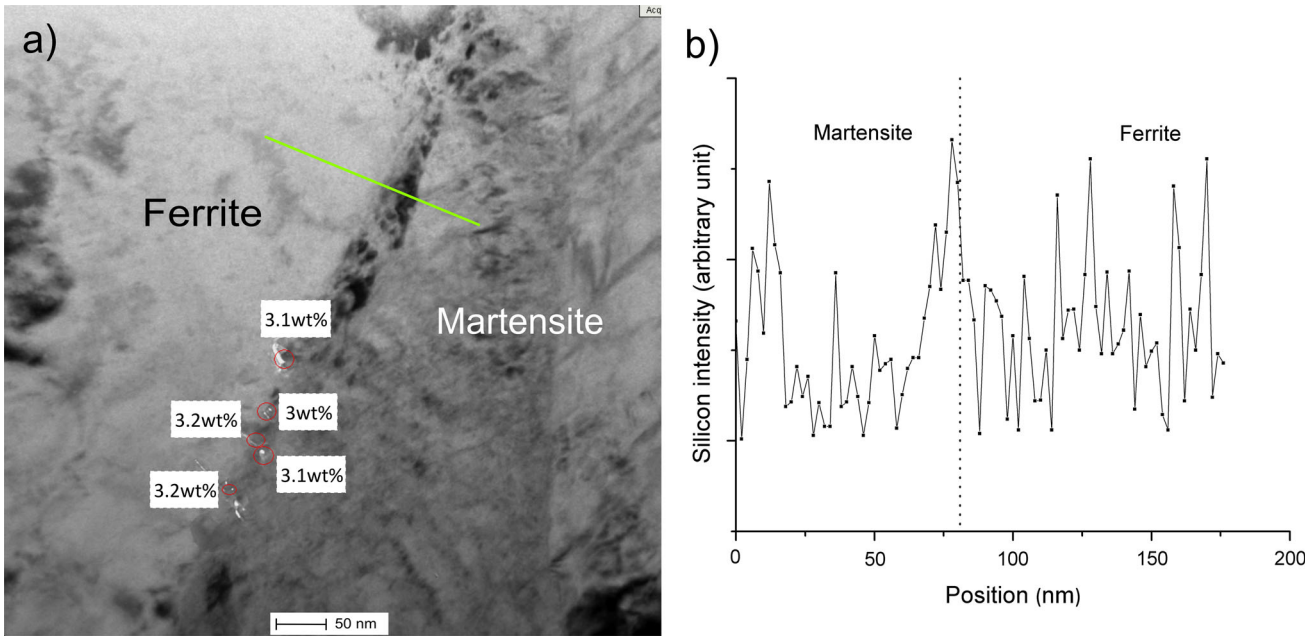

Fig. 8—Sample quenched from 775 °C: (*a*) bright-field image; (*b*) intensity.

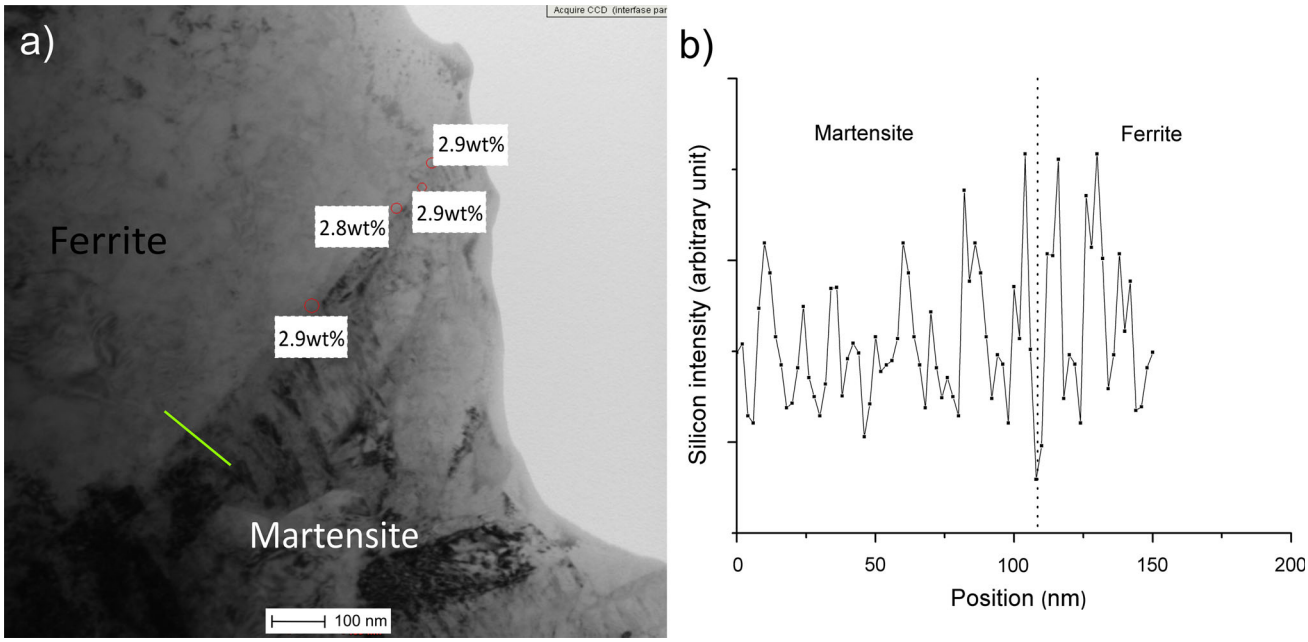

Fig. 9—Sample quenched from 760 °C: (*a*) bright-field image; (*b*) intensity.

transformation, the microsegregation developed during the solidification must be accounted for in the analysis of the austenite transformation upon cooling. This is especially important at the FTF, where the ferritic transformation is known to start from. As a result, new diagrams should be introduced to study the ferritic transformation in SGI, not only taking into account the PE mode governing its growth but also accounting for the change in the local concentration of alloying elements as the ferrite interface advances.

Figure 12 shows two examples of pseudobinary equilibrium diagrams and the PE diagram overlapped. Both

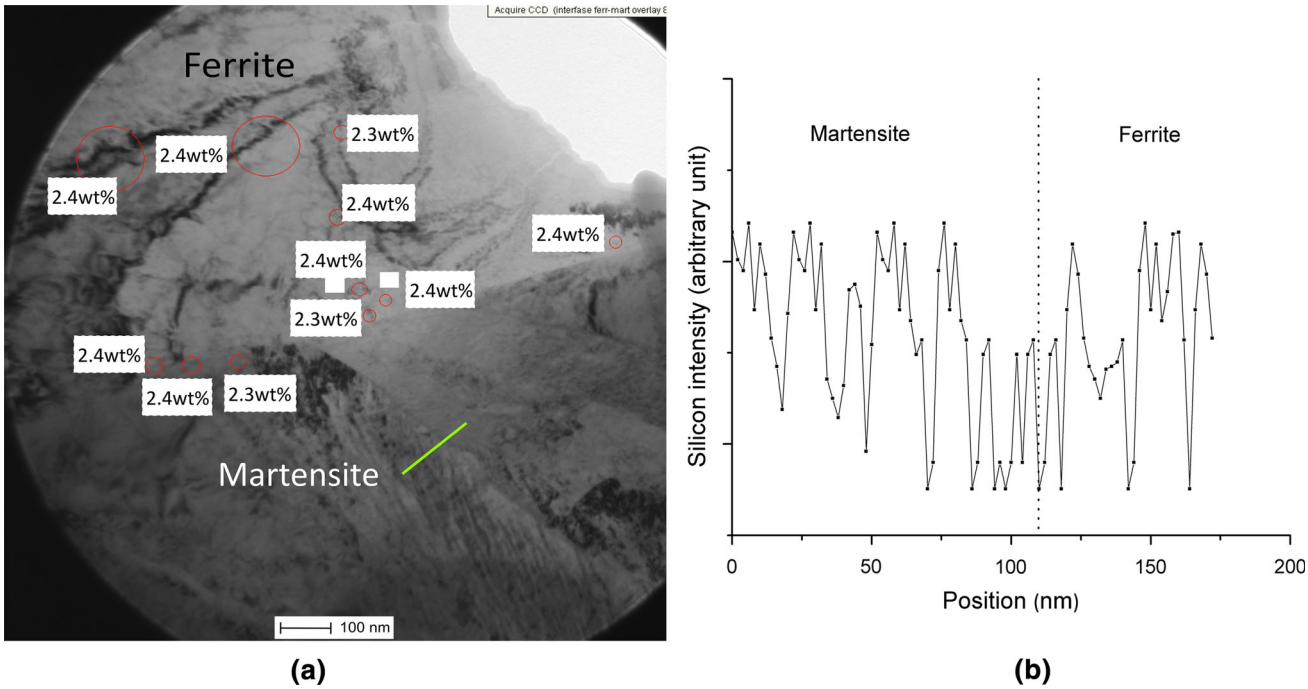

Fig. 10—Sample quenched from 745 °C: (*a*) bright-field image; (*b*) intensity.

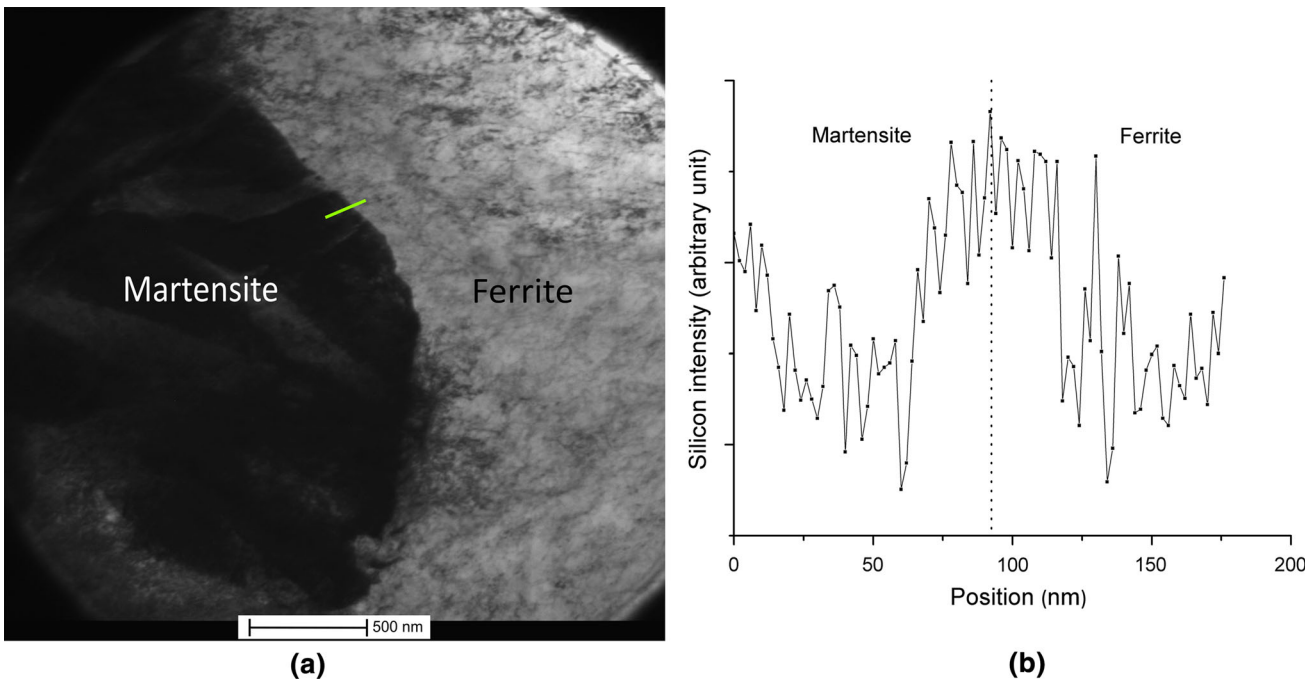

Fig. 11—Sample quenched from 730 °C: (*a*) bright-field image; (*b*) intensity.

were generated using the Thermo-Calc software[16] and TCFE8 database. The first one is for a Si concentration of 3.2 wt pct and the second one is for a concentration of 1.9 wt pct. These Si concentrations represent the averaged compositions measured at the FTF and LTF in the alloy studied in this work (Figure 5). The C supersaturation at the temperature measured for the beginning of the ferritic transformation with DSC (777 °C) is shown on the first plot, both for equilibrium (ΔC_C) and PE (ΔC_C PE) diagrams. At the same temperature, the Si-depleted regions do not show carbon supersaturation.

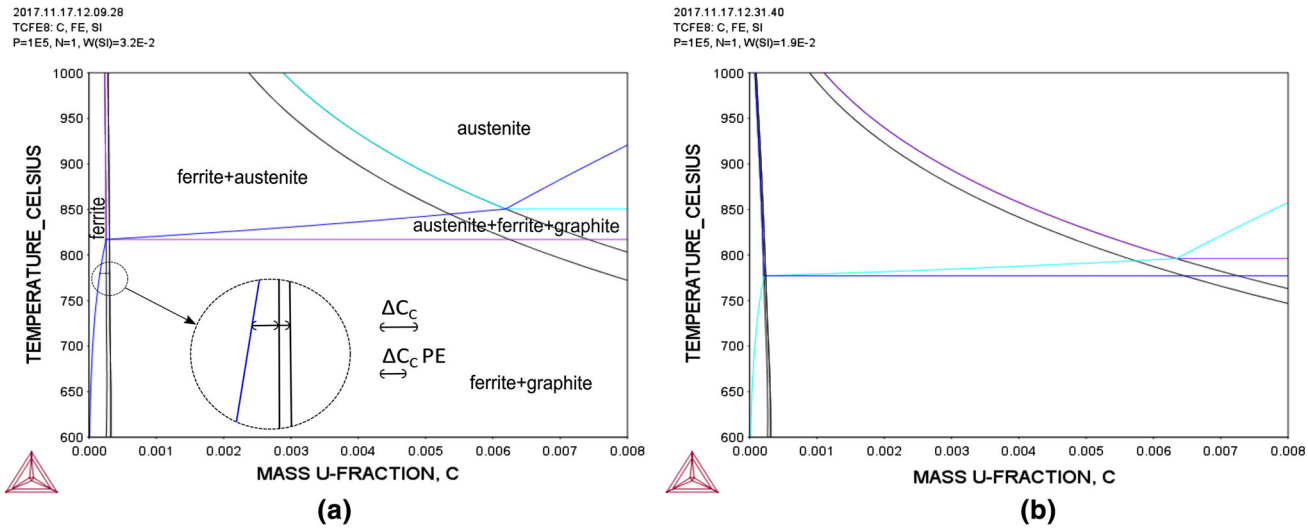

Fig. 12—Fe-C-Si isopleth sections: (*a*) 3.2 wt pct Si; (*b*) 1.9 wt pct Si.

The C supersaturation varies with the Si concentration, and therefore the driving force for nucleation and growth of ferrite is greater at the higher Si concentration regions. Consequently, it is clear that nucleation will begin at these locations. At a constant temperature, the driving force for ferrite growth will decrease as the interface approaches lower Si concentration areas in the austenite matrix. As a result, cooling is necessary for ferrite growth to continue.

In conclusion, assuming the average Si concentration for the analysis of the driving force for ferrite growth would be an error. Rather, multiple PE isopleth sections should be considered if the transformation is to be accurately described: one for each point of the austenite matrix, accounting for the alloying element profiles developed during the solidification.

IV. CONCLUSIONS

This work clarified the transformation mode ruling ferrite precipitation from austenite in SGI. The results of careful microanalysis across the interfaces between growing ferrite and austenite showed no signs of the presence of a Si concentration spike. Therefore, the possibility of growth under a NPLE mode has been dismissed. Instead, the results support the conclusion that ferrite precipitation develops with no partition of the alloying elements under a PE mode.

For the comprehensive modeling of ferritic growth in SGI, the driving force for C diffusion should be calculated considering PE diagrams. This has a clear consequence on the driving force for the ferritic growth, which also varies with the Si concentration considered for its calculation. As the austenite matrix has inherited the Si profiles developed during solidification, the change in Si concentration as the transformation front advances must be accounted for by the PE diagrams. Modeling the ferrite growth including these conclusions would be the next step.

ACKNOWLEDGMENTS

The authors would like to thank the Sánchez and Piccioni Company for providing them its facilities to carry out the casts and Dr. Tolley (CAB-CNEA) for his help with the TEM measurements. L.N. García, F.D. Carazo, and R.E. Boeri are members of CONICET and would like to thank the institution for the economic support for their respective researches. L.N. García would like to especially thank the SECITI (Secretaría de Estado de Ciencia, Tecnología e Innovación del Gobierno de San Juan) and the INP school for the economic support for her stay at the CIRIMAT laboratory at Toulouse, France. Finally, L.N. García would like to deeply thank Prof. Jacques Lacaze for transmitting his knowledge about Thermo-Calc software and for enriching the discussions of this research.

REFERENCES

1. J. Lacaze, C. Wilson, and C. Bak: *Scand. J. Metall.*, 1994, vol. 23, pp. 151–63.
2. V. Gerval and J. Lacaze: *ISIJ Int.*, 2000, vol. 40, pp. 386–92.
3. D.E. Coates: *Metall. Mater. Trans. B*, 1973, vol. 4, pp. 1077–86.
4. M. Wessen and I.L. Svensson: *Metall. Trans. A*, 1996, vol. 27A, pp. 2209–20.
5. R. Boeri and F. Weinberg: *AFS Trans.*, 1989, vol. 97, pp. 179–84.
6. J. Lacaze, J. Sertucha, and L. Magnusson Åberg: *ISIJ Int.*, 2016, vol. 56, pp. 1606–15.
7. X. Guo and D. Stefanescu: *Int. J. Cast Met. Res.*, 1999, vol. 11, pp. 437–42.
8. A. Freulon, P. de Parseval, C. Josse, J. Bourdie, and J. Lacaze: *Metall. Trans. A*, 2016, vol. 47A, pp. 5362–71.
9. D. Stefanescu: *Metall. Trans. A*, 2017, vol. 48A, pp. 2127–29.
10. J. Lacaze: *Metall. Trans. A*, 2017, vol. 48A, pp. 2130–31.
11. G. Rivera, R. Boeri, and J.A. Sikora: *Cast Met*, 1995, vol. 8, pp. 1–5.

12. L.N. García, F.D. Carazo, and P.M. Dardati: *Int. J. Cast. Met. Res*, 2018, vol. 31, pp. 209–21.
13. ASTM A536-84(2019)e1, Standard Specification for Ductile Iron Castings, ASTM International, West Conshohocken, PA, 2019, www.astm.org.
14. R. Ivanova, W. Sha, and S. Malinov: *ISIJ Int.*, 2004, vol. 44, pp. 886–95.
15. L.A. Currie: *Anal. Chim. Acta*, 1999, vol. 391, pp. 127–34.
16. J.O. Andersson, T. Helander, L. Höglund *et al.*: *Calphad*, 2002, vol. 26, pp. 273–312.